Table -3, Figure - 22, Page -23

Supplementary Information

The following information is provided to the article on

"Unbiased solar H_2 production with current density up to 23 mA/cm^2 by swiss-cheese black Si coupled with wastewater bioanode"

Lu Lu,[1,5,†] Waltteri Vakki,[2,†] Jeffery A. Aguiar,[3] Chuanxiao Xiao,[4] Katherine Hurst,[4] Michael Fairchild[2], Xi Chen,[1] Fan Yang[2], Jing Gu,[2]* Zhiyong Jason Ren[1,5]*

[1] Department of Civil, Environmental, and Architectural Engineering, University of Colorado Boulder, Boulder, Colorado 80309, USA.

[2] Department of Chemistry and Biochemistry, San Diego State University, 5500 Campanile Drive, San Diego, California 92182, USA

[3] Idaho National Laboratory, Nuclear Materials Department, 2525 Fremont Avenue, Idaho Falls, Idaho 83415, USA

[4] National Renewable Energy Laboratory, Chemistry and Nanoscience Center, Golden, Colorado 80401, USA.

[5] Department of Civil and Environmental Engineering and Andlinger Center for Energy and the Environment, Princeton University, Princeton, NJ 08544

*Corresponding author e-mail: jgu@sdsu.edu, zjren@princeton.edu

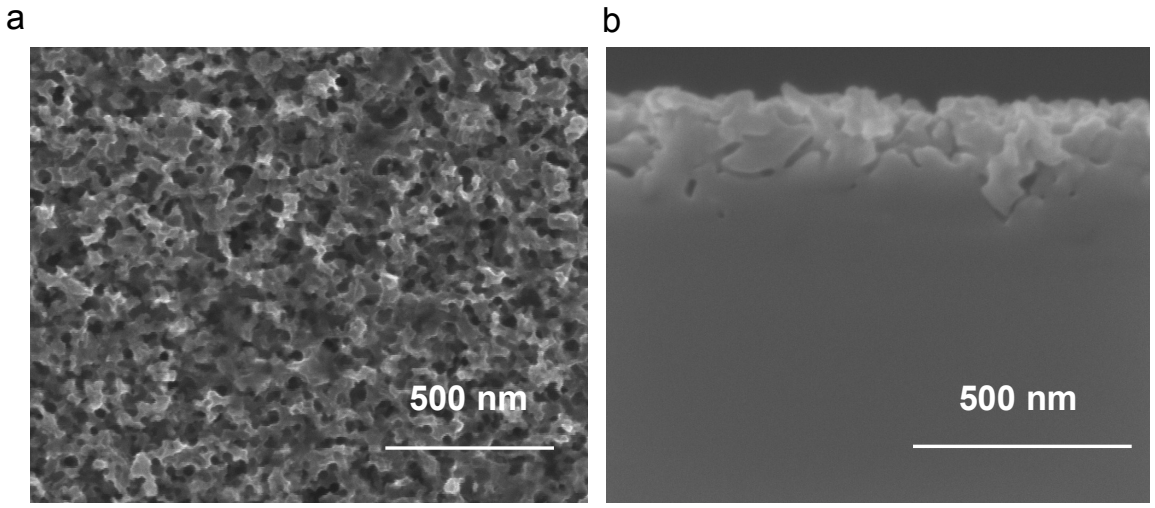

Fig. S1. SEM images of unmodified black silicon electrode. (**a**) planar view (**b**) cross section view.

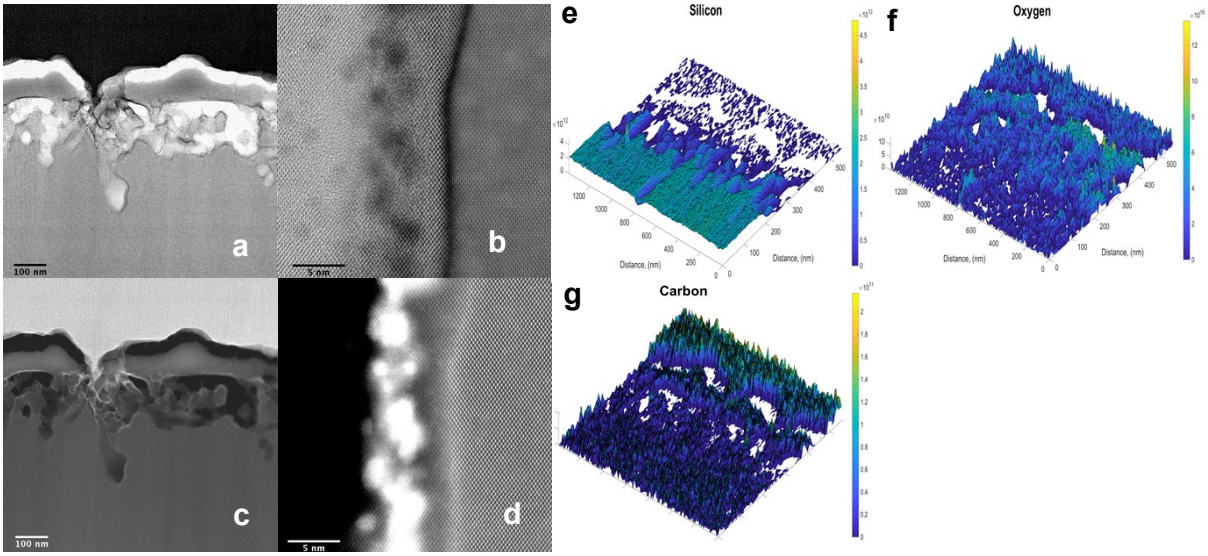

Fig. S2. Detailed Chemistry and Structure of b-Si/ MoS_x interface. Collecting a (**a**) bright and (**b**) simultaneous dark field STEM image presents the over distribution of MoS_x that decorate the tops of the silicon wafer. A higher magnification image looking cross section of $MoS_x/SiO_x/Si$ STEM images as (**c**) bright and (**d**) dark field imaging reveals an amorphous feature of MoS_x layer and SiO_x layer on top of B-Si. Over the same field of view, energy filtered EELS reveal the distribution of (**e**) silicon, (**f**) oxygen, (**g**) carbon.

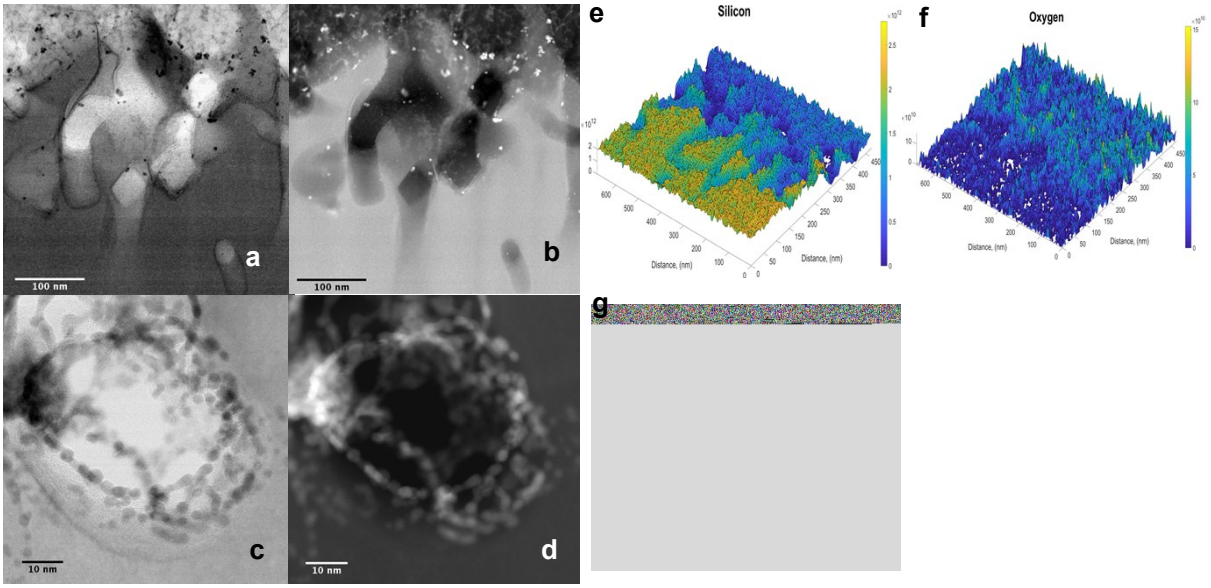

Fig. S3. Detailed Chemistry and Structure of b-Si/Pt interface. Collecting a (**a**) bright and (**b**) simultaneous dark field STEM image presents the over distribution of platinum bright particles that decorate the walls of the silicon wafer. A higher magnification image looking perpendicular to a tunnel, using STEM (**c**) bright and (**d**) dark field imaging reveals an amorphous inner tunnel layer. Over the same field of view, energy filtered EELS reveal the distribution of (**e**) silicon, (**f**) oxygen, (**g**) carbon.

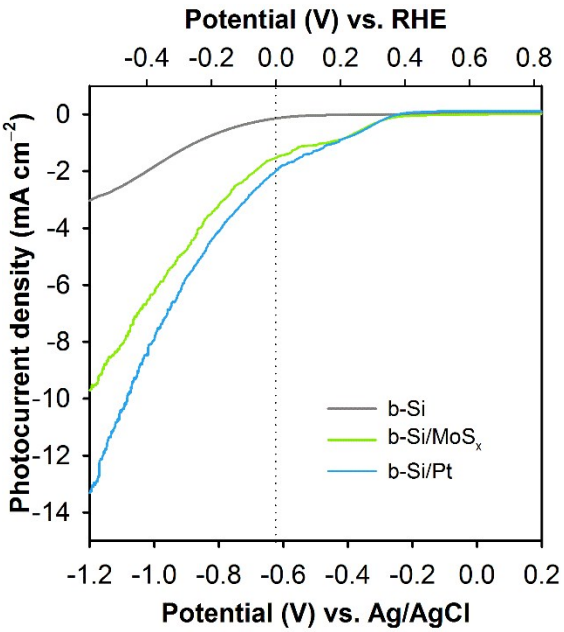

Fig. S4. *J-V* curves of b-Si-based photocathode under neutral condition. Scan was conducted at a rate of 10 mVs^{-1} in 0.2 M phosphate buffered solution (PBS) (pH 7.0) under 1 sun illumination.

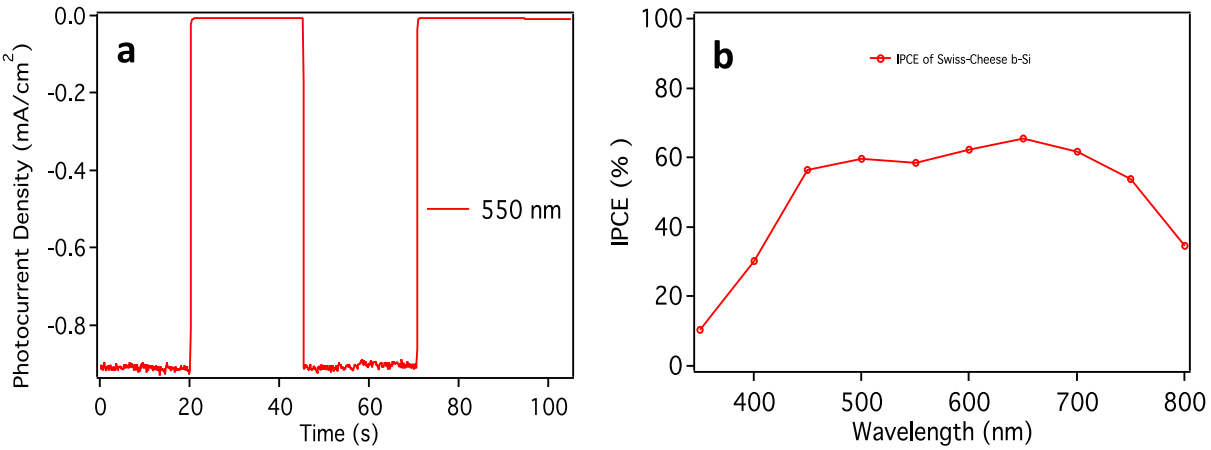

Fig S5. The IPCE experiment was carried out in an electrochemical cell using a 300 W Xe arc-lamp and band pass filters. (**a**) Sample data is shown here using a 550 nm filter. (**b**) The IPCE of the swiss-cheese b-Si electrode under -0.6 V vs. Ag/AgCl in 0.2 M H_2SO_4.

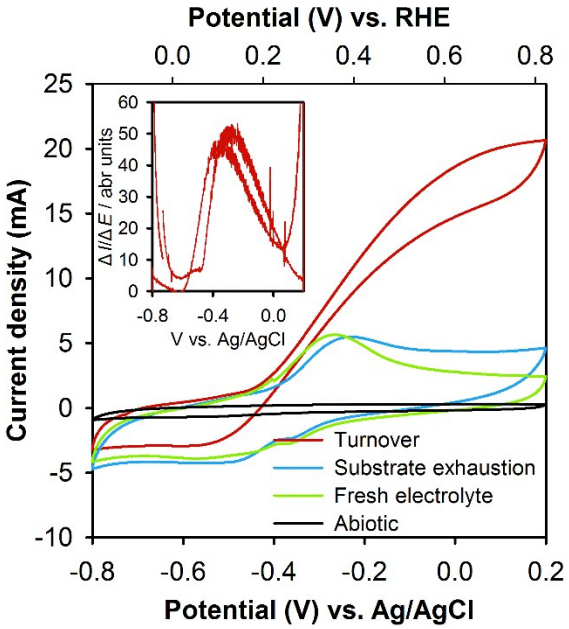

Fig. S6. Cyclic voltammogram (CV) of bioanode fed with artificial wastewater (AW). CV were conducted under turnover condition (red line) at maximum biofilm activity and non-turnover conditions with substrate exhaustion (blue line) or in a fresh electrolyte without substrate (green line). The scan rate was 5 mVs^{-1}. An abiotic anode was also scanned as control (black line). Inset: first derivatives of the turn-over CV.

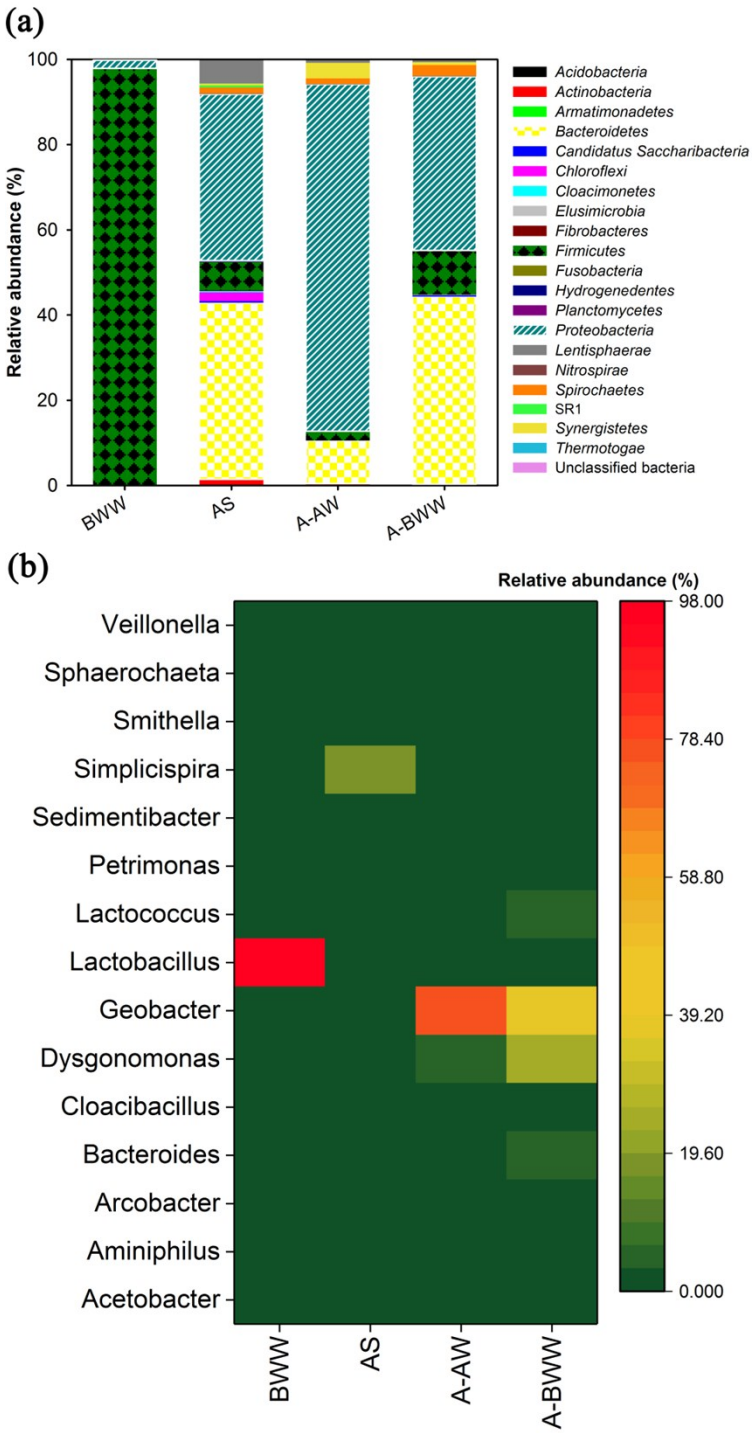

Fig. S7. Taxonomic classification of bacterial DNA sequences. Samples were collected from communities of brewery wastewater (BWW), anaerobic sludge (AS) inoculum and bioanode fed with artificial wastewater (A-AW) and brewery wastewater (A-BWW) at the (**a**) phylum level and (**b**) genus level. Relative abundance was defined as the number of sequences affiliated with that phylum and genus divided by the total sequence number of per sample. The genera that are less than 1% of total composition in all libraries were ignored in heatmap graph.

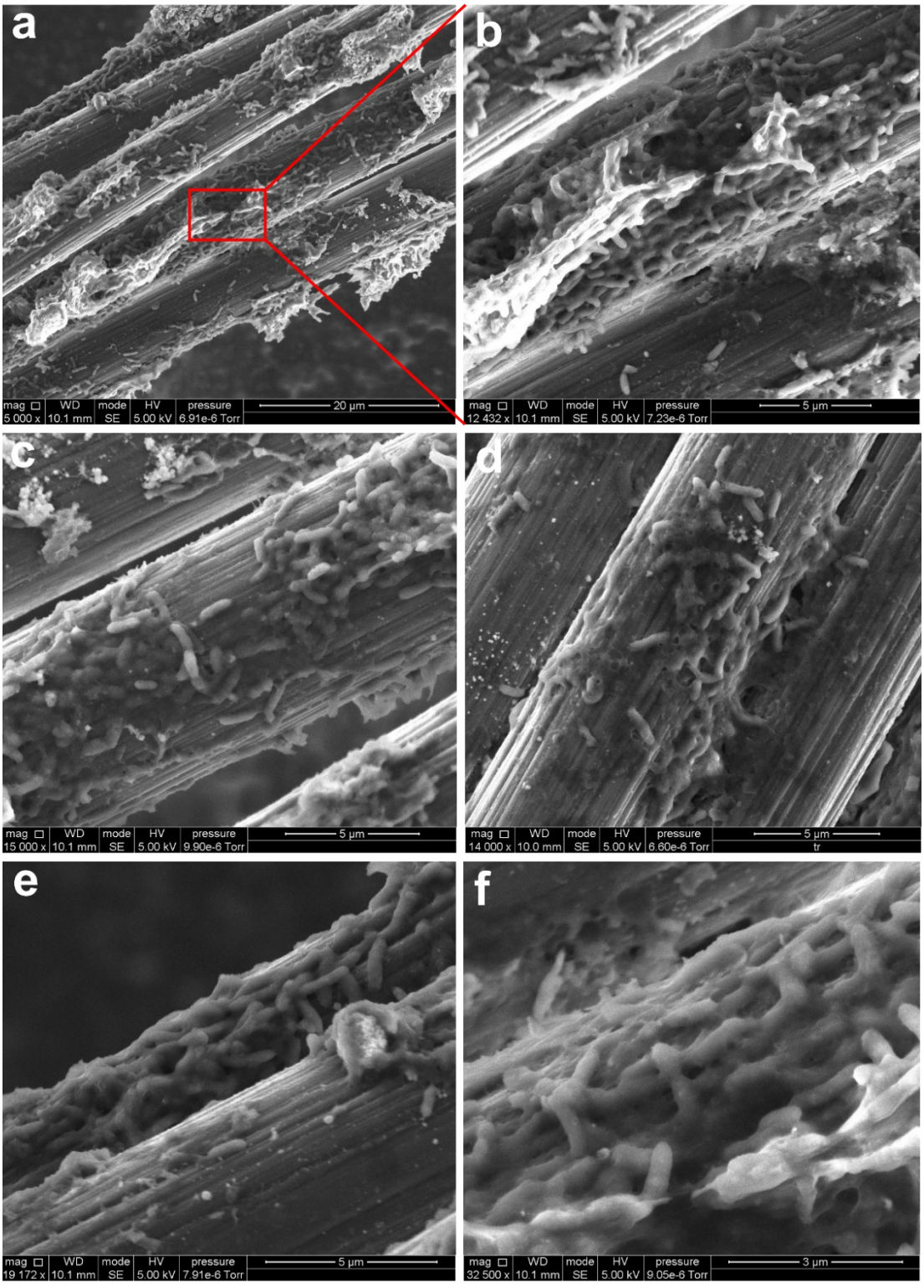

Fig. S8. (**a**)-(**f**) SEM images of the electroactive biofilm grown on the carbon fiber anode. (**b**) Magnified image of red area in (**a**). SEM images confirm that bacteria tightly colonize on the surface of solid carbon fibers.

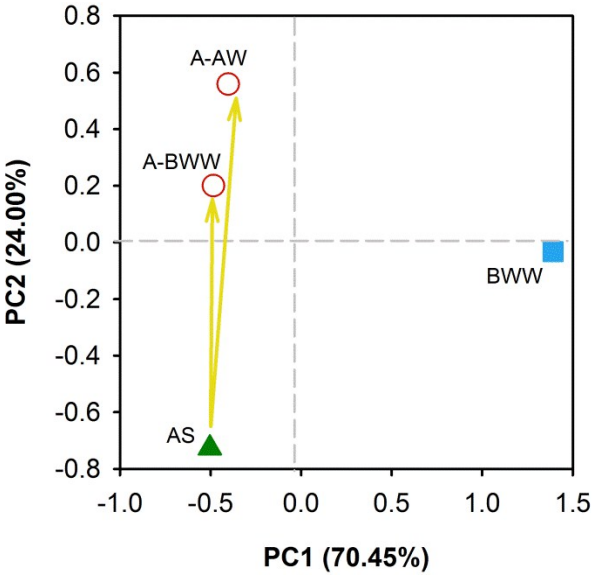

Fig. S9. Weighted Fast UniFrac Principal Coordinates Analysis (PCoA) of bacterial communities. PCoA shows a dramatical shift of microbial community structures of brewery wastewater (BWW), anaerobic sludge (AS) inoculum and bioanode fed with artificial wastewater (A-AW) and brewery wastewater (A-BWW).

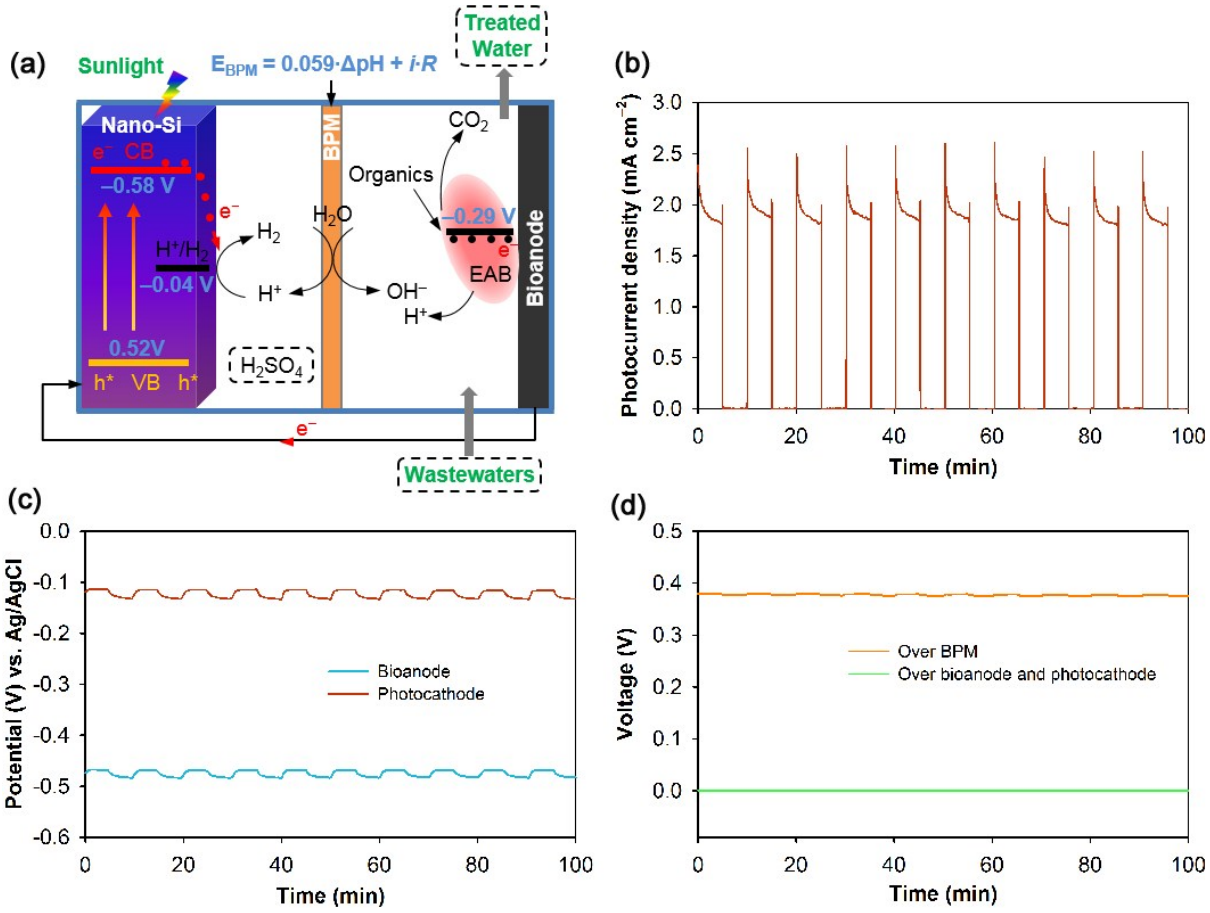

Fig. S10. Self-sustaining MPEC by coupling one bioanode and one b-Si/MoS_x photocathode. (**a**) Schematic of MPEC device. The thermodynamic potentials (vs. NHE) of H^+/H_2 and organics oxidation by EAB, band edges of CB and VB under zero bias, and a voltage drop over the bipolar membrane (E_{BPM}) were indicated. (**b**) photocurrent density-time (*J*-*t*) curves, (**c**) electrode potentials of MPEC. (**d**) measured voltages drop over bipolar membrane, and voltage over bioanode and photocathode. MPEC reactor was fed with brewery wastewater (BWW) and under 1 sun on/off illumination.

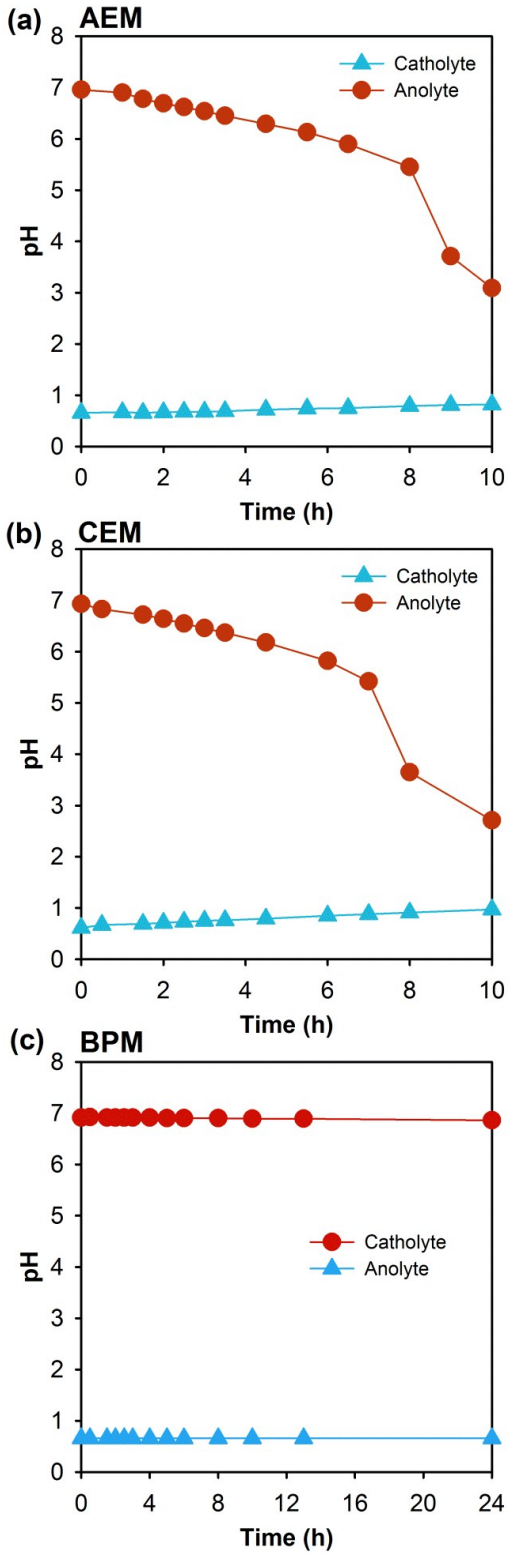

Fig. S11. Changes in electrolyte pH as a function of time. Anolyte is 0.2 M phosphate buffered solution and catholyte is 0.2 M H_2SO_4. Both electrolytes were separated by a bipolar membrane (BPM).

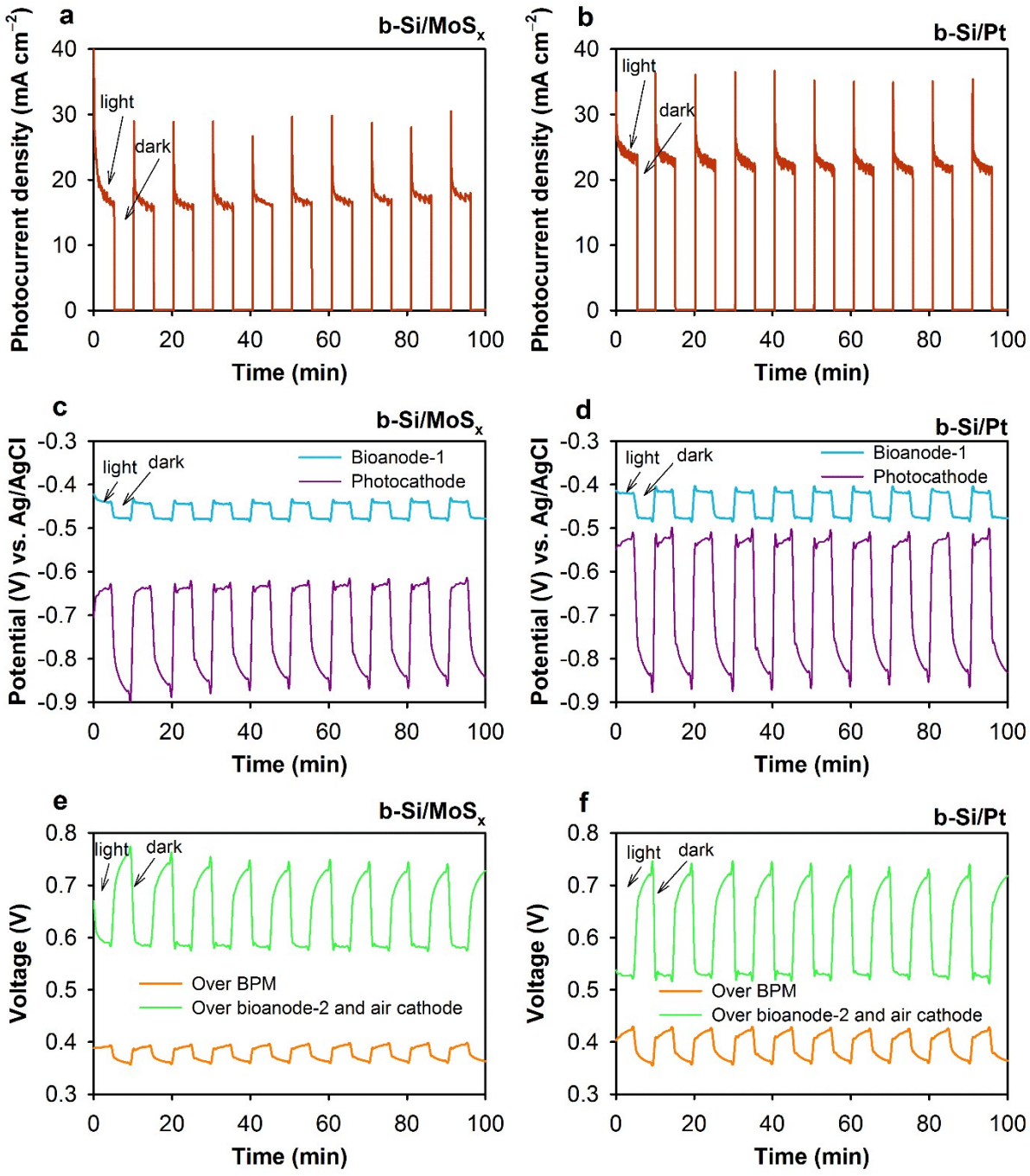

Fig. S12. Characterization of MPEC fed with artificial wastewater (AW) under 1 sun on/off illumination. (**a**) and (**b**), Photocurrent density-time (*J-t*) curves. (c) and (d), Electrode potentials of MPEC. **e**, **f**, Voltage drop over bipolar membrane (BPM), and voltage over bioanode-2 and air cathode that serves as a bias for photocathode. MPEC was fed with artificial wastewater (AW).

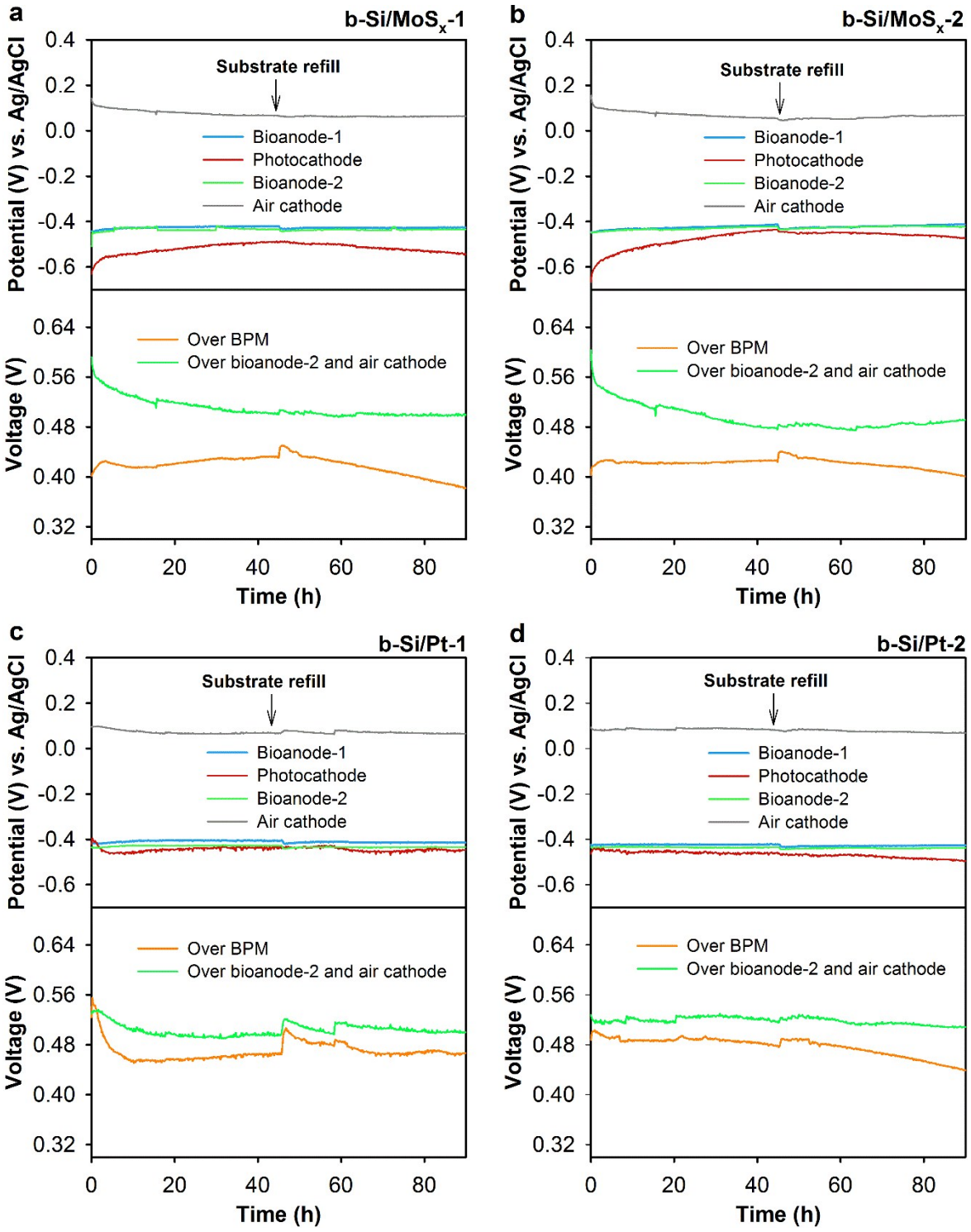

Fig. S13. Potentials of each MPEC component. Electrode potentials, voltage drop over bipolar membrane (BPM), and voltage over bioanode-2 and air cathode that serves as a bias for photocathode during 90 h long-term operation of MPEC device fed with brewery wastewater (BWW).

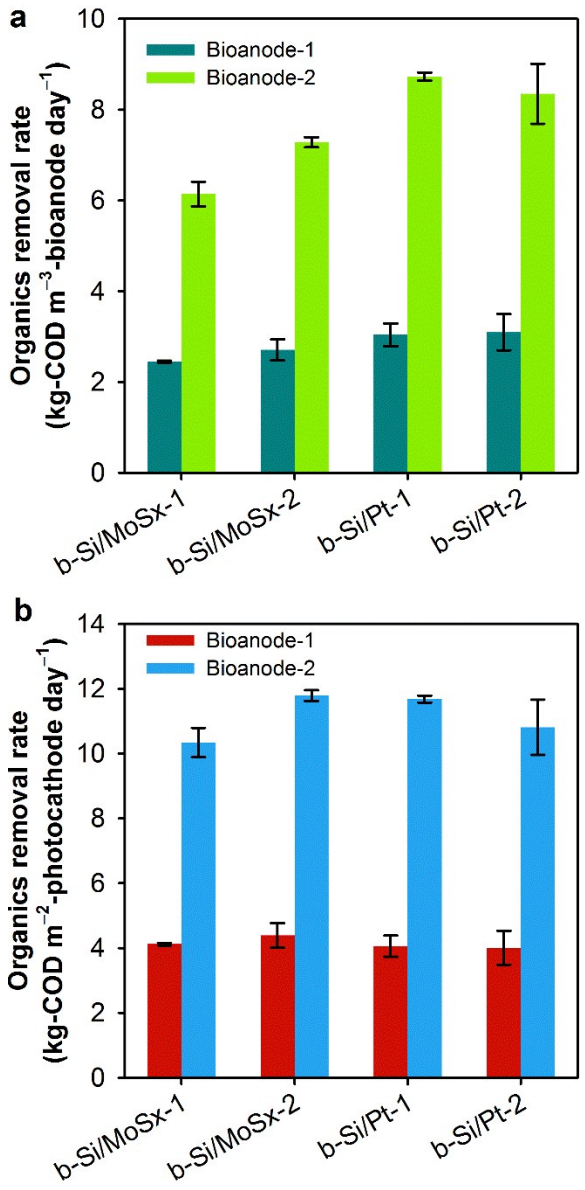

Fig. S14. Organics removal by MPEC. The removal rate was normalized to (**a**) bioanode volume and (**b**) photocathode area. Duplicate experiment was conducted by using two similar photocathodes named "1" and "2".

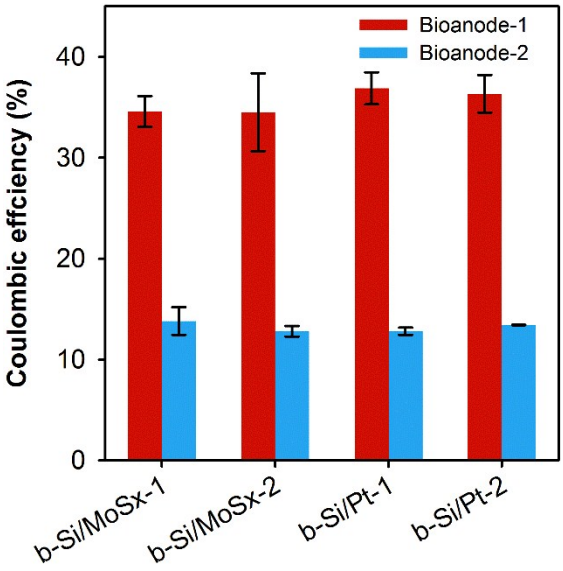

Fig. S15. Coulombic efficiencies in MPEC. Duplicate experiment was conducted by using two similar photocathodes named "1" and "2".

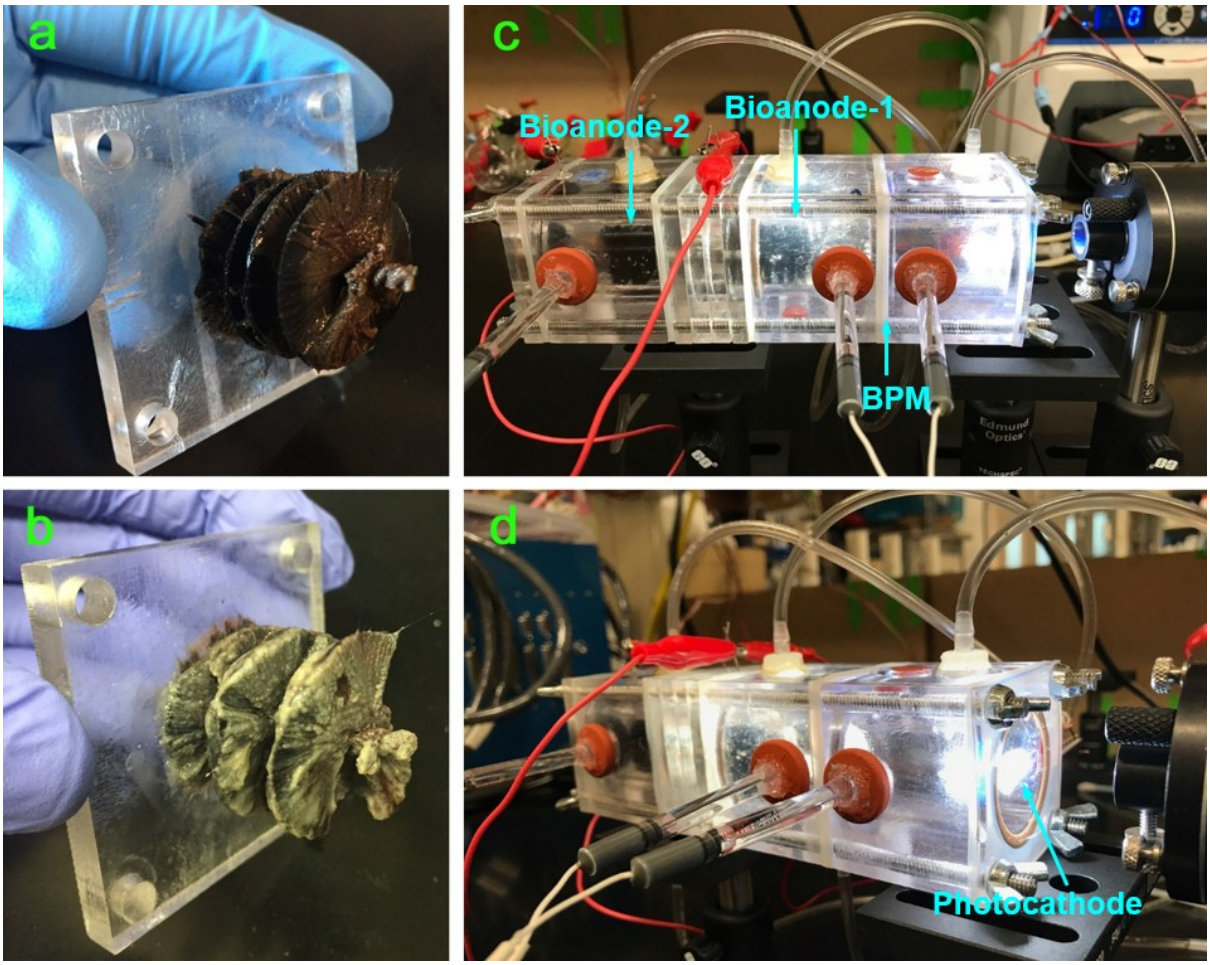

Fig. S16. Digital images of MPEC reactor. Bioanode fed with (**a**) artificial wastewater (AW) and (**b**) brewery wastewater (BWW), (**c, d**) MPEC reactor.

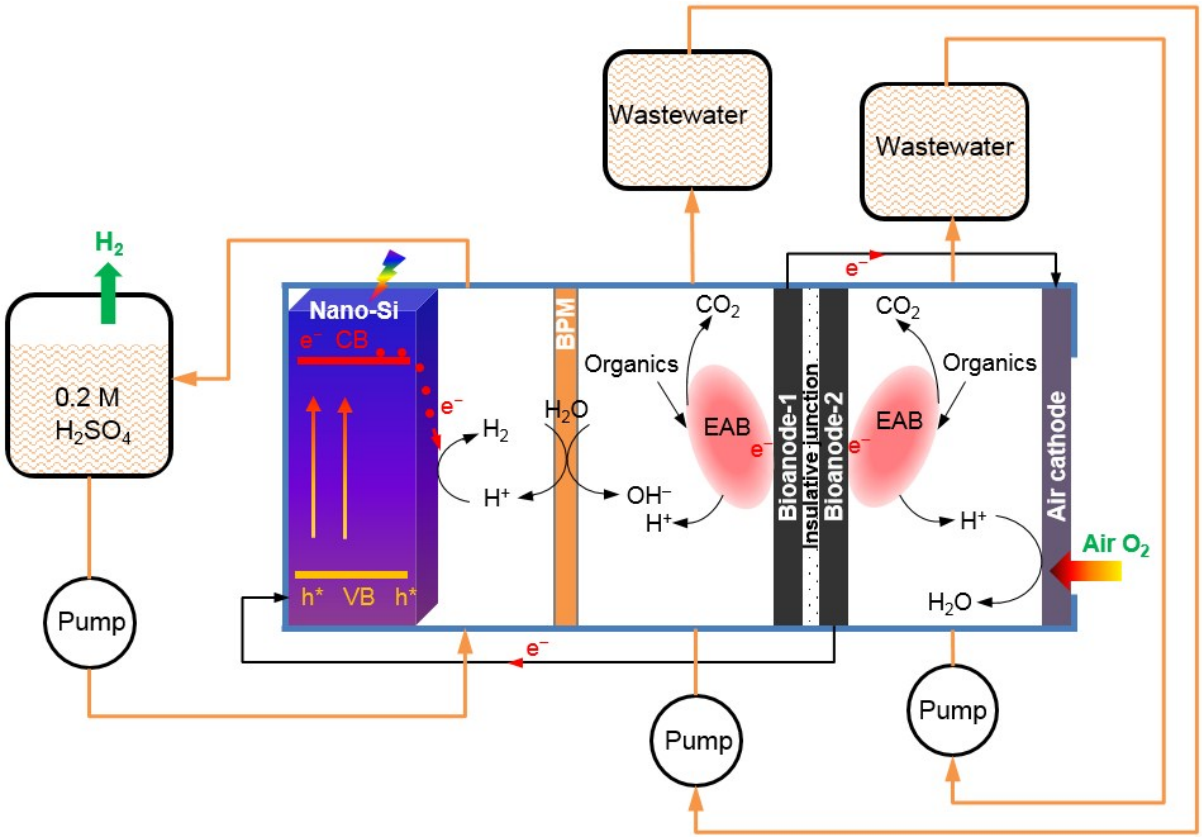

Fig. S17. Schematic of operating process of MPEC device.

Fig. S18. Screenshot of H_2 generation from MPEC. Video clip is attached.

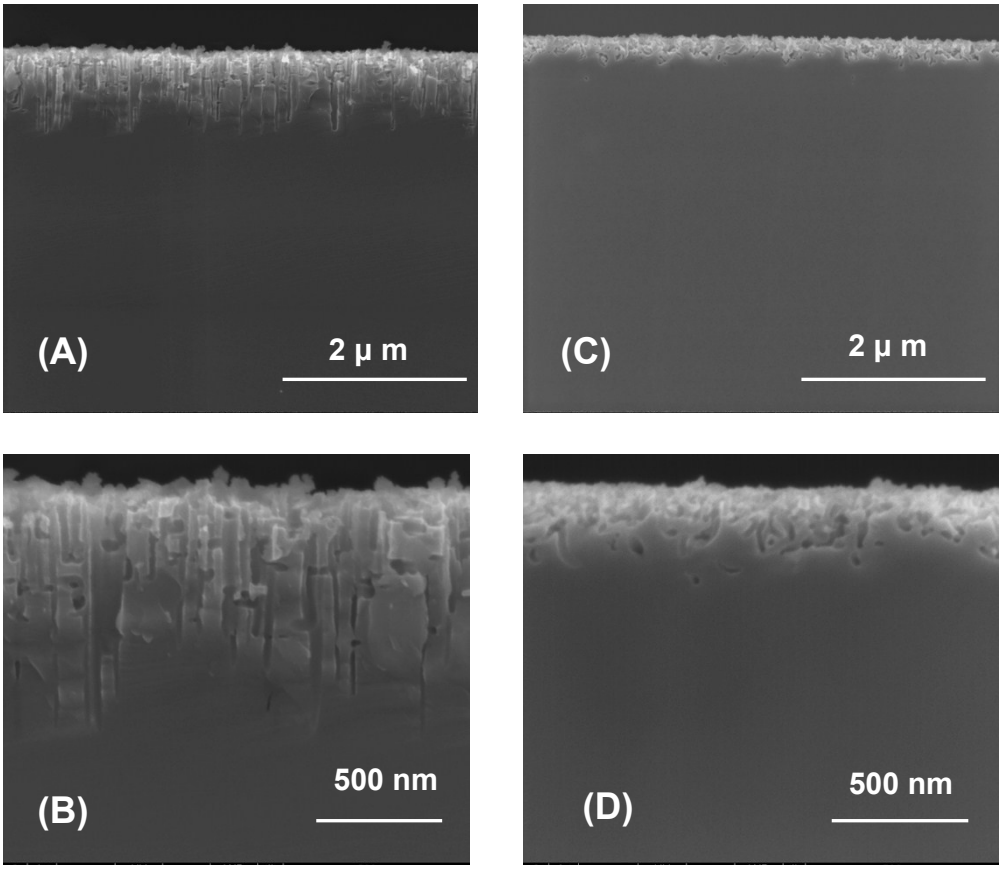

Fig. S19. SEM images of the b-Si with different interface. Conventional column (**a and b**) and swiss cheese interface b-Si (**c and d**).

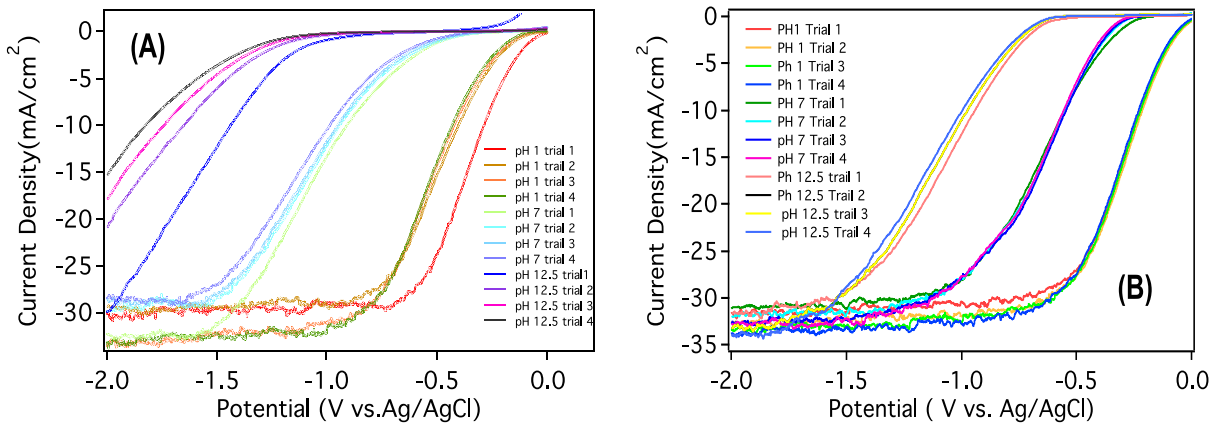

Fig. S20. Stability test of the b-Si with different interface. pH stability test of the column (**a**) and swiss cheese black silicon (**b**) at pH 1(0.1 M H_2SO_4), pH 7 (phosphate buffer) and pH 12.5 (0.1 M NaOH).

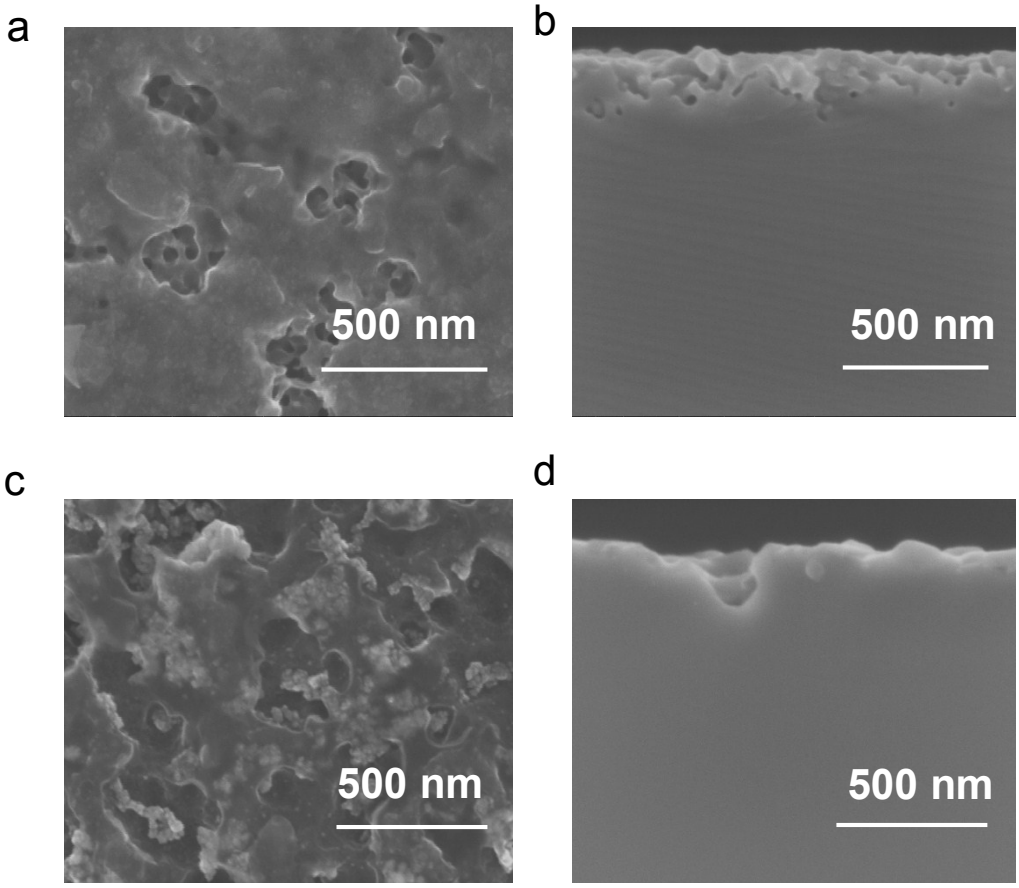

Fig. S21. Planar and cross section SEM images of photocathodes after electrolysis. (**a,b**) b-Si/MoS_x electrode after 90 h electrolysis (**c,d**) b-Si/Pt electrode after 90 h electrolysis.

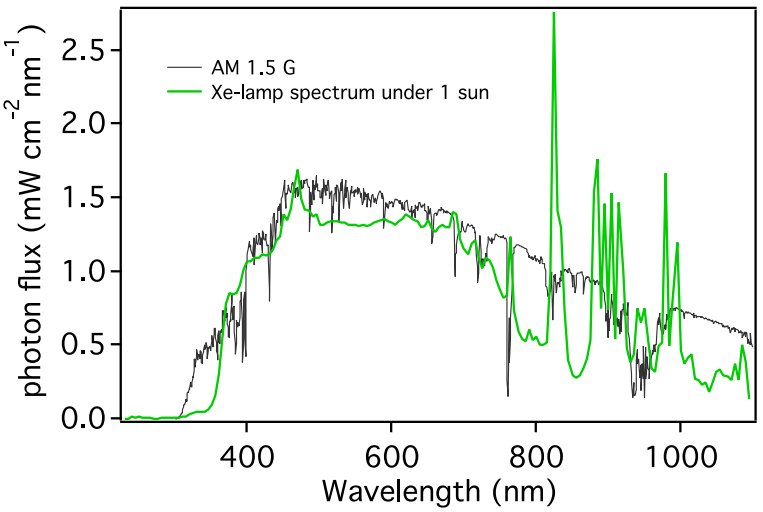

Fig. S22. The spectrum of Xe-arc lamp under 1 sun (100 mW/cm^2) condition with the AM 1.5G standard spectrum.

Calculations of Coulombic and Faradaic Efficiencies

All calculations are based on long-term (90 h) experiments.

The theoretical moles of H_2 (n_{CE}) that could be recovered based on the measured current is,

$$n_{CE} = \frac{\sum_{i=1}^{n} I_i \Delta t}{2F} \qquad (1)$$

Where, Δt is the interval (0.1 second in this study) over which current data are collected, and F= 96485 C/mol-electron is Faraday's constant. Each mole of H_2 generation will need two moles of electrons.

Since all electrons used for H_2 production are derived from organics, the theoretical maximal moles of H_2 generation (n_{th}) could be calculated based on substrate consumption using measured chemical oxygen demand (COD) data.

$$n_{th} = \frac{2\Delta \mathrm{COD}}{M_{O_2}} \qquad (2)$$

Where, $\Delta \mathrm{COD}$ (g) is the cumulative COD consumption over a period of time. M_{O_2} (32 g/mol) is the molecular weight of oxygen. Each mole of COD removal will produce 2 moles of H_2.

The Coulombic efficiency (C_E , %) indicated a substrate to current conversion efficiency is,

$$C_E = \frac{n_{CE}}{n_{th}} \quad (3)$$

The Faradaic efficiency (FE, %) indicated a current to H_2 conversion efficiency is,

$$FE = \frac{n_{H_2}}{n_{CE}} \quad (4)$$

Table S1. Summary of PEC performance of Si-Pt and Si-MoS_x photoelectrodes.

	Catalyst loading amount (nmol)	**Total charge (C)**	**TON**	**TOF**	**TON average for two electrodes**	**TOF average for two electrodes**
Si-Pt 1	8.74	641.5	380301	1.17	388768.5	1.20
Si-Pt 2	9.72	745.2	397236	1.23		
Si-MoS_2 1	5.42	518.4	495573	1.53	495471.5	1.53
Si-MoS_2 2	6.10	583.2	495370	1.53		

Table S2. Comparison of state-of-the-art conventional photoelectrochemical (PEC) systems and microbial photoelectrochemical (MPEC) system in this study for self-sustaining H_2 production. (1 sun illumination except noted).

Light Absorber	Current Density (mA/cm^2)	STH (%)	Stability (hour)	Reference
$GaInP_2$/GaAs tandem solar cell	10 (1 sun) and 120(12 sun)	12.4	0.5	Science, 1998,280, 425-427
3jn-a-Si/Co-OEC with Ni/NiMoZn	3	2.5(wireless) and 4.7(wired)	< 1	Science, 2011, 334, 645-648
Si Pillars/Mo_3S_4	9	10	1	Nature Materials, 2011, 10, 434-438
CoO nanoparticles	-	5	1	Nature Nanotechnology, 2013, 9 ,69
p-GaN/p-$In_{0.2}Ga_{0.8}N$ nanowires	-	1.8	10	Nature Communication, 2015, 6, 6797
$BiVO_4$/WO_3/DSSC	4.5	5.7	2	Nano. Energy. 2015, 13, 182-191
$BiVO_4$/WO_3 with DSSC/TiO_2	5.5	7	10	Nature Communication, 2016, 7, 11943
InGaP/GaAs/GaInNAsSb triple junction solar cell	25	30	50	Nature Communication, 2016, 7, 13237
GaInP/GaInAs tandem absorber	13	16	0.33	Nature Energy, 2017, 2, 17028
Cu_2O/Ga_2O_3/TiO_2/RuO_x coupled with n-$BiVO_4$	2.5	3	100	Nature Catalysis, 2018, 1, 412-420
PV-PEC tandem n^+np^+-Si photocathode with p^+pn^+ Si photoanode	5	9.8	100	J. Mater. Chem. A. 2019, DOI:10.1039/C8TA10165E
Bioanode with Si-MoS_x	**21-24**	**-**	**90**	**This work**

Table S3. Experimental photo-flux and photocurrent density values for swiss-cheese b-Si and transmission of the round bottom flask are used to calculate final IPCE at a given wavelength.

Wavelength	Photo Flux(mW/cm^2)	Photocurrent (mA/cm^2)	IPCE%, Before calibration	Transmission of cell with 0.2 M H_2SO_4	IPCE%, After calibration
350 nm	0.654	0.015	8.12	0.794	10.2
400 nm	1.28	0.107	26.1	0.861	30.3
450 nm	2.36	0.412	48.2	0.851	56.6
500 nm	3.38	0.706	51.7	0.867	59.6
550 nm	3.94	0.916	52.4	0.895	58.6
600 nm	4.03	1.06	54.5	0.873	62.4
650 nm	4.14	1.22	56.3	0.859	65.6
700 nm	5.30	1.61	53.8	0.87	61.9
750 nm	8.92	2.27	42.1	0.78	54.0
800 nm	9.88	1.76	27.6	0.8	34.6